Nano Research
2023, 16(9): 11885–11892

ISSN 1998-0124 CN 11-5974/O4
https://doi.org/10.1007/s12274-023-5722-y

Research Article

Coaxial fiber organic electrochemical transistor with high transconductance

Yuan Fang, Jianyou Feng, Xiang Shi, Yiqing Yang, Jiajia Wang, Xiao Sun, Wenjun Li, Xuemei Sun (✉), and Huisheng Peng (✉)

State Key Laboratory of Molecular Engineering of Polymers, Department of Macromolecular Science, and Laboratory of Advanced Materials, Fudan University, Shanghai 200438, China

Received: 31 January 2023 / **Revised:** 14 March 2023 / **Accepted:** 9 April 2023

ABSTRACT

Fiber organic electrochemical transistors (OECTs) have received extensive attention in wearable and implantable biosensors because of their high flexibility and low working voltage. However, the transconductance of fiber OECTs is much lower compared with the planar counterparts, leading to low sensitivity. Here, we developed fiber OECTs in a coaxial configuration with microscale channel length to achieve the highest transconductance of 135 mS, which is one to two orders of magnitude higher than that of the state-of-the-art fiber OECTs. Coaxial fiber OECT based sensors showed high sensitivities of 12.78, 20.53 and 3.78 mA/decade to ascorbic acid, hydrogen peroxide and glucose, respectively. These fiber OECTs were woven into a fabric to monitor the glucose in sweat during exercise and implanted in mouse brain to detect ascorbic acid. This coaxial architectural design offers an effective way to promote the performance of fiber OECTs and realize highly sensitive detection of biochemicals.

KEYWORDS

organic electrochemical transistor, fiber, coaxial structure, ascorbic acid, hydrogen peroxide, glucose

1 Introduction

Flexible fiber biosensors have attracted wide attention in wearable and implantable applications, because they can be woven into textiles or implanted into tissues to detect the chemicals in body fluids such as sweat, urine and blood [1–3]. Among them, fiber organic electrochemical transistors (OECTs) based sensors have unique advantages of *in situ* amplification for the detected signals and low working voltages, and thus have been developed to detect various biochemicals, such as dopamine [4], glucose [5] and ions [6]. However, the transconductances that determine the amplification ability of fiber OECTs are generally one to two orders of magnitude lower than that of planar OECTs [7–9]. The low transconductance leads to low detecting sensitivity, which limits the further application of fiber OECTs in biochemical sensing.

The transconductance of OECT is proportionate to the decreased channel length and increased channel width according to the Bernards model [10], as OECT is intrinsically composed of conductive polymer channel between source and drain electrodes. On this basis, the high transconductances of planar OECTs have been reported with micrometer-scale channel length [11] and millimeter-scale channel width in interdigital architecture [12] by patterning the geometries of source and drain electrodes through high-precision photolithography. While fiber OECTs were usually fabricated by depositing the source and drain electrodes at two ends of the fiber and then patterning the conductive polymer channel between them [13, 14]. However, it is difficult to precisely pattern electrodes and polymers in micron sizes on highly curved fiber surface by using the existing microfabrication methods. Therefore, it is urgent but difficult to obtain high transconductances for fiber OECTs.

In this work, we reported a fiber OECT in coaxial architecture showing a record transconductance of 135 mS. The coaxial fiber OECT was fabricated by depositing the drain electrode, conductive polymer channel and Au network source electrode layer by layer on the fiber surface. The channel length was decided by the thickness of the conductive polymer layer, which was reduced to ~ 5 μm. The carbon nanotube (CNT) fiber was used as the gate electrode due to its low bending stiffness, larger specific surface area, high structure stability under deformations and easy modification for detection of various chemicals compared with other electrodes such as Pt and Au wires [13, 15, 16]. Through the modification of CNT fiber gate, the fiber OECT based sensors showed high sensitivity for multiple biochemicals and high stability in deformation and body fluid soaking. The coaxial fiber OECT was woven into a wrister to detect the glucose concentration in sweat during exercise and implanted into the mouse brain for the detection of ascorbic acid (AA), demonstrating the potential application as wearable and implantable devices.

2 Results and discussion

The fiber OECT consists of a coaxial channel fiber and a CNT fiber gate (Figs. 1(a) and 1(b)). To construct the coaxial channel fiber, 5 nm Cr and 100 nm Au were deposited onto the nylon fiber with a diameter of 180 μm as the drain electrode, followed by

Address correspondence to Xuemei Sun, sunxm@fudan.edu.cn; Huisheng Peng, penghs@fudan.edu.cn

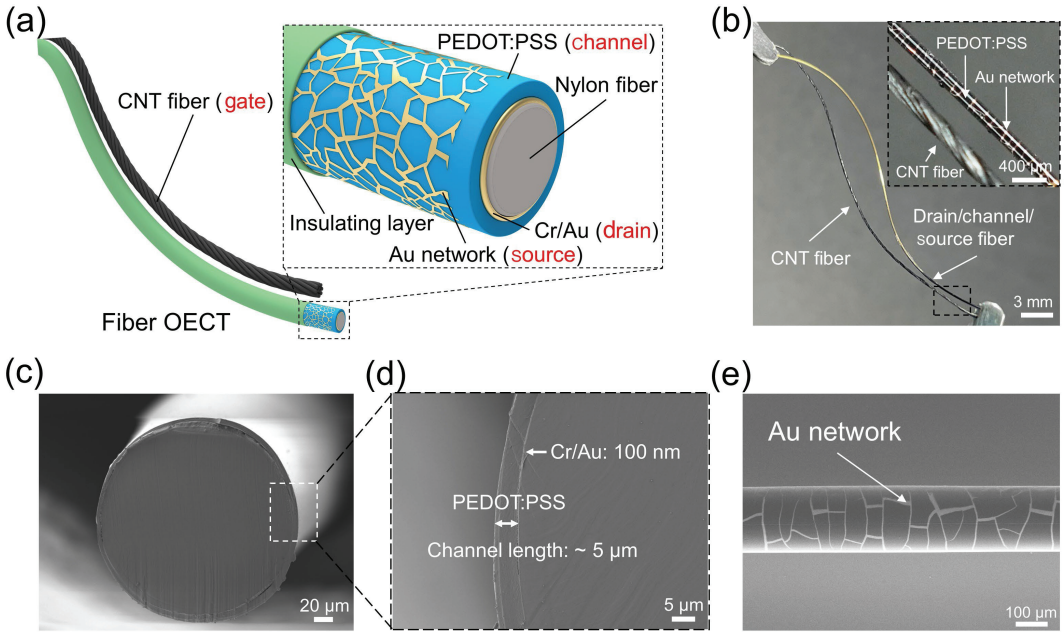

Figure 1 The structure of coaxial fiber OECTs. (a) Schematic illustration of coaxial fiber OECT. (b) Photo of coaxial fiber OECT. The inset picture is the enlarged view of the coaxial fiber OECT. (c) Cross-sectional SEM image of coaxial nylon fiber with PEDOT:PSS/Cr/Au coating. (d) Local amplification of (c) showing the channel length of PEDOT:PSS layer. (e) SEM image of Au network deposited on PEDOT:PSS layer.

coating of poly(3,4-ethylenedioxythiophene)-poly(styrenesulfonate) (PEDOT:PSS) layer as the conductive polymer channel in the thickness of ~ 5 μm (Figs. 1(c) and 1(d)). In order for ions in the electrolyte to migrate into the PEDOT: PSS layer, Au network was constructed at the out surface as the source electrode (Fig. 1(e)). A lift-off process was used to fabricate the Au network (Figs. S1 and S2 in the Electronic Supplementary Material (ESM)) based on the dip-coated crackle template. The crackle template was made of the acrylic resin colloid. First, the waterborne acrylic resin colloidal dispersion was coated on the fiber and formed a uniform film. Then, in the process of film drying, the capillary pressure generated by water evaporation drove the acrylic resin film to contract, while the shear stress from the fiber substrate resisted this contraction. Therefore, the in-plane stress in the film was finally released in the form of cracks [17, 18]. And then Au was evaporated onto the cracks. The grid density of the Au network ranging from ~ 100 to ~ 500 mm^{-2} could be controlled by the dip-coating rate of the crackle template (Figs. S3(a)–S3(d) in the ESM). The increasing dip-coating speed led to a thicker crackle template layer with larger crack spacing and width [19], resulting in Au network with lower grid density but larger line width (Fig. S3(e) in the ESM). The minimum resistance of the Au network of 200 Ω/cm was achieved at ~ 150 mm^{-2} grid density (Fig. S3(f) in the ESM). This was because the resistance was affected by both the conductive paths and line width. With the increase of grid density, the number of conductive paths increased to reduce resistance, while the line width decreased to lead to the increase of resistance [20]. When the two factors reached a balance, the resistance was minimum. Owing to the special network structure, the Au network electrode also exhibited electrical stability under different deformation. The resistance showed less than 3% change after bending, twisting and friction against tissue-mimicking gels for 1000 times (Figs. S4 and S5 in the ESM).

Due to the coaxial architecture, the hole carriers were transported from the outer layer to the internal layer across the PEDOT:PSS layer. When a positive gate bias was applied, cations from the electrolyte solution migrated into the PEDOT:PSS layer through the Au network (Fig. S6 in the ESM). Then, the cations de-doped the $PEDOT^+$ by compensating the PSS^- to maintain the electrical neutrality in the PEDOT:PSS layer at steady. The number of holes in the channel was reduced, resulting in a decrease of drain current (Fig. 2(a)). The output and transfer characteristics of coaxial fiber OECTs showed typical depletion-type curves (Figs. 2(b) and 2(c)). When the gate voltage scanned from 0 to 0.8 V, the drain current was modulated for over three orders of magnitude, from the on-state current of 34 mA to the off-state current of 24 μA (Fig. 2(c) and Fig. S7 in the ESM). Besides, the response time was 0.85 s and the drain current response maintained stable and reversible in 100 cycles (Fig. S8 in the ESM).

According to the Bernards model, transconductance is inversely proportional to the channel length. It indicates that a small channel length is beneficial to a high transconductance. Different from the traditional co-planar structure, the channel length of this coaxial structure was decided by the thickness of PEDOT:PSS layer, and can be easily adjusted by changing the coating parameters. Here we realized a channel length of ~ 5 μm through multiple solution coating, to our best knowledge, which is the smallest value for fiber OECTs (Fig. 2(d)). Besides, PEDOT:PSS layer of micron thickness can also effectively avoid the short circuit between the drain and source electrodes. As a result, the coaxial fiber OECT exhibited the highest transconductance of 135 mS at the gate voltage of 0.27 V (Fig. 2(c)), which is almost 10 times greater than the transconductances of the previously reported fiber OECTs (Fig. 2(d)) [21].

In practical applications, the performance of coaxial fiber OECTs should keep mechanically and chemically stable. The mechanical stability under bending and friction was achieved by network structure to reduce stress concentration and Cr intermedium layer between Au and PEDOT:PSS for strong interfacial bonding (Fig. S9 in the ESM). The coaxial fiber OECTs were proved to be highly stable under different bending radii from 10 to 1.5 mm and cyclic bending for 500 times in terms of transconductance, on-state current, and on-off current ratio (Fig. 2(e) and Fig. S10 in the ESMs). Frictions inevitably occurred between coaxial fiber OECTs and human tissues whether in wearable or implantable applications. We used hydrogels in different moduli that simulated brain, muscle and skin to evaluate the friction stability of the devices. The transfer and transconductance curves were in high coincidence before and after

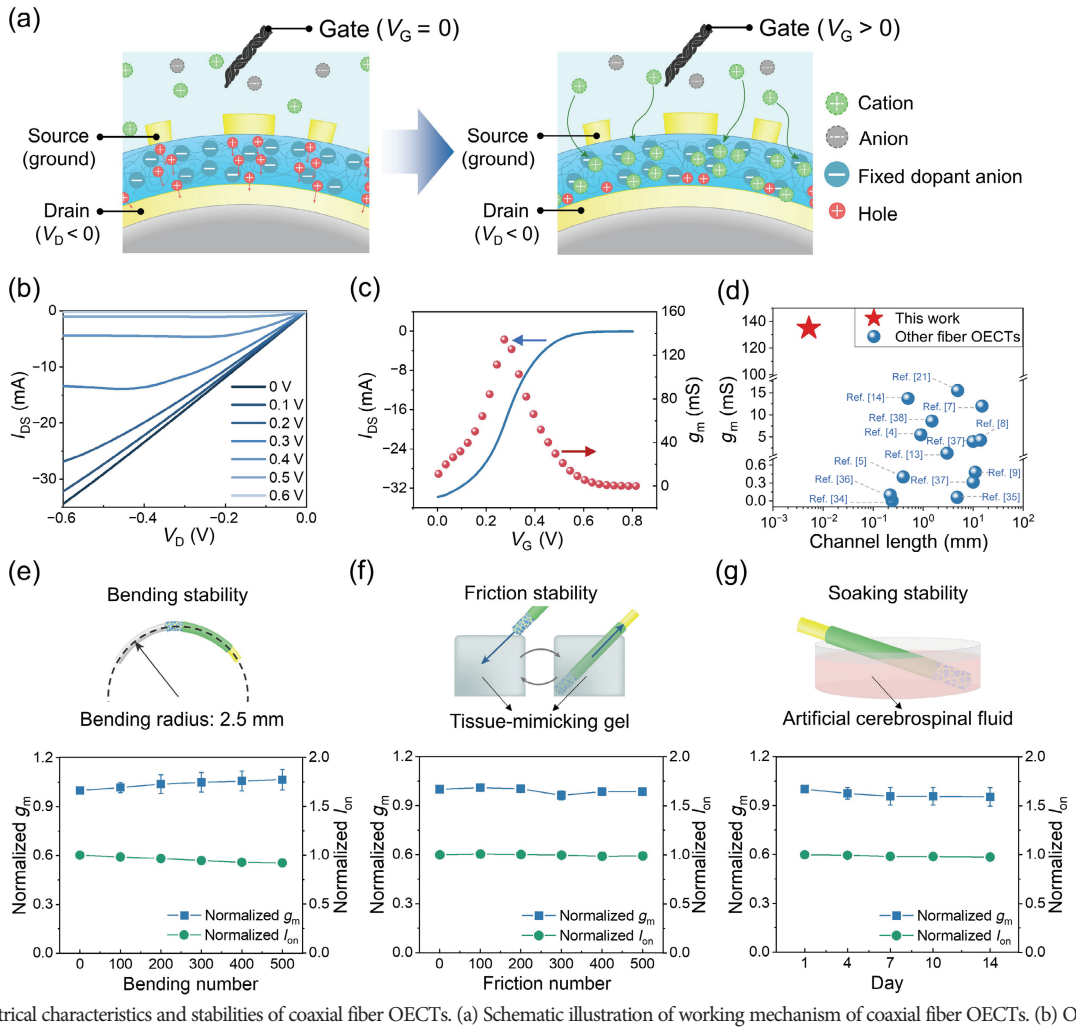

Figure 2 Electrical characteristics and stabilities of coaxial fiber OECTs. (a) Schematic illustration of working mechanism of coaxial fiber OECTs. (b) Output curves of the OECTs using 0.01 M PBS as the electrolyte. (c) Transfer (solid line) and transconductance (sphere symbol) curves of the OECTs using 0.01 M PBS as the electrolyte measured at V_D = −0.6 V. (d) Maximum transconductance and channel length for coaxial fiber OECTs and other previously reported fiber OECTs [4, 5, 7–9, 13, 14, 21, 34–38]. (e) Normalized transconductance and on-state current under 500 bending times with a bending radius of 2.5 mm. (f) Normalized transconductance and on-state current under 500 friction times in tissue-mimicking gel. (g) Normalized transconductance and on-state current during 14 days in artificial cerebrospinal fluid.

friction (Fig. S11 in the ESM), and the decrease of on-state current and the transconductance was less than 2% after rubbing against the tissue-mimicking gel for 500 times (Fig. 2(f)). Furthermore, the outer source electrode based on inert Au offered a good chemical stability for the long-term soaking in body fluids. After 14-day soaking in artificial cerebrospinal fluid, the on-state current and transconductance of coaxial fiber OECTs varied less than 5% (Fig. 2(g)).

Besides the coaxial channel fibers, the impedance of the CNT fiber gate also remained stable after repeated bending, friction and 14-day soaking (Figs. S12 and S13 in the ESM). High transconductance combined with mechanical and chemical stability indicated that coaxial fiber OECTs could be made into stable biochemical sensors with high sensitivity. Taking advantage of the easy multi-functionalization of CNT fiber gates, a series of biosensors based on coaxial fiber OECTs were prepared to detect different chemicals, including electrochemically active molecules, electrochemically inactive molecules and metabolic intermediates.

AA is an indispensable chemical substance in the human body associated with metabolic diseases and mental illness [22]. Since the CNT fiber has notable catalytic activity for AA, the coaxial fiber OECT with a bare CNT fiber gate was used to detect AA. When a voltage of 0.2 V was applied to the CNT fiber gate, AA was oxidized to dehydroascorbic acid and the electrons were transferred to the CNT fiber (Fig. 3(a)). Then the oxidation reaction raised the electrolyte potential, promoting cation migration into the PEDOT:PSS layer, resulting in the decrease of drain current (Fig. S14 in the ESM) [23]. As shown in Fig. 3(b), the coaxial fiber OECT displayed a linear response with the logarithm of the concentration of AA in the range of 0.1–1 mM, which was close to the concentration of AA in human tissue [24]. The sensitivity was 12.78 mA/decade and the limit of detection was 1 μM (Fig. S15 in the ESM).

Hydrogen peroxide (H_2O_2) is widely used as an intermediate for biochemical sensing, such as glutamate [25] and glucose [26]. Platinum (Pt) nanoparticles (NPs) that are catalytically active on H_2O_2 were electrodeposited on the CNT fiber to fabricate the gate electrode. Complete coverage of Pt NPs on CNT fibers was realized by electroplating for 0.08 C (Figs. S16(a) and S16(b) in the ESM). Under the gate voltage of 0.2 V, H_2O_2 was catalyzed by Pt NPs into O_2, and electrons flowed from H_2O_2, causing the rise of electrolyte potential, leading to the reduction of the drain current (Fig. 3(c) and Fig. S16(c) in the ESM). The sensitivity was 20.53 mA/decade with a linear range of 0.02–0.2 mM (Fig. 3(d)).

Glucose is the primary source of energy in the human body, which plays an important role in cellular metabolic processes [27]. The real-time monitoring of glucose is significant in reducing the risk of metabolic diseases such as diabetes. The CNT fiber was modified with tetrathiafulvalene (TTF) as the electron transfer agent and the glucose oxidase (GOx) as the catalyst for the glucose-sensing gate (Figs. S17(a) and S17(b) in the ESM). Glucose was oxidized into gluconolactone and the electron was transported

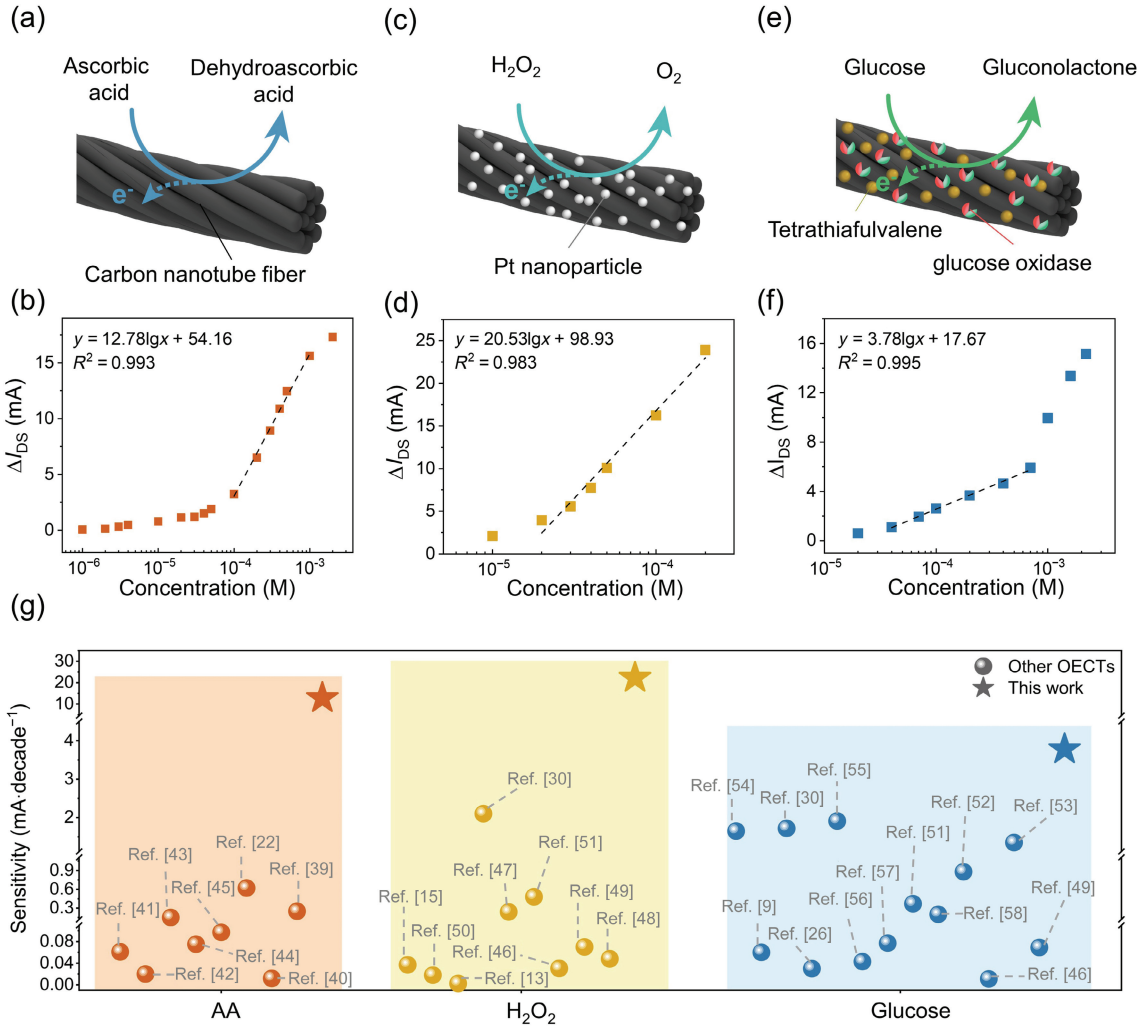

Figure 3 High sensitivity of coaxial fiber OECT based biosensors. (a) Schematic illustration for CNT fiber gate electrode and the mechanism of AA detection. (b) Drain current change in function of AA concentration. (c) Schematic illustration for H_2O_2 sensing fiber gate electrode and the mechanism. (d) Drain current change in function of H_2O_2 concentration. (e) Schematic illustration for glucose sensing fiber gate electrode and the mechanism. (f) Drain current change in function of glucose concentration. The black dotted line is the linear fitting curve of drain current change to concentration. (g) Sensitivity of biosensors based on coaxial fiber OECTs and other reported OECTs for detecting AA [22, 39–45], H_2O_2 [13, 15, 30, 46–51] and glucose [9, 26, 30, 46, 49, 51–58]. In all cases, coaxial fiber OECTs are operated at $V_D = -0.6$ V and $V_G = 0.2$ V.

from the GOx redox center to the CNT fiber via TTF (Fig. 3(e)) [28]. The sensitivity of glucose detection was 3.78 mA/decade (Fig. 3(f)). The limit of detection was 20 μM. The linear range spanned from 0.04 to 0.7 mM, which covered the concentration of glucose in human sweat (0.06 mM to 0.2 mM) (Fig. S17(c) in the ESM) [29]. The sensitivities of AA, H_2O_2, and glucose were improved by over 20, 10 and 2 times respectively compared with the previously reported OECTs (Fig. 3(g) and Tables S1, S2, and S3 in the ESM) [22, 30].

These fiber OECT based sensors exhibited high sensitivity and flexibility, which were suitable for integration into wearable fabrics to monitor sweat in real time. Therefore, we then wove the coaxial fiber OECT with a glucose-sensing fiber gate into a cotton wrister for real-time monitoring of sweat glucose concentration (Fig. 4(a)). Compared with other chemicals in sweat, such as sodium (Na^+), potassium (K^+), ammonium (NH_4^+), lactate and uric acid (UA), the fiber OECT based glucose sensor has a more obvious current response to glucose (Fig. 4(b)) [31]. The real-time monitoring of sweat glucose was performed when a volunteer wearing the OECT-woven wrister was cycling indoors (Fig. 4(c)). During the 20-min cycling, the concentration of sweat glucose decreased from 102 to 86 μM, which was consistent with the fact that glucose was consumed during the exercise [32]. Besides, the data of *in-situ* detection based on coaxial fiber OECT were verified by using the commercial enzyme-based glucose sensor to detect the sweat samples collected after cycling for 25, 35 and 45 min (Fig. 4(d)).

Because of the small size and one-dimension structure of coaxial fiber OECTs, they could also be implanted into brains for chemical sensing. Then the coaxial fiber OECT with an unmodified CNT fiber gate was implanted in the deep brain of mice to detect AA (Fig. 4(e)). A 6 mA variation of the drain current was observed ($V_G = 0.2$ V, $V_{DS} = -0.6$ V) when 2 μL of AA solution (5 mM) was injected into the brain with a microsyringe (Fig. 4(f)). In the control group, the drain current didn't change after injecting normal saline. The selectivity *in vivo* was also investigated by injecting dopamine (DA) and glucose in the same concentration as AA. Compared with AA, the responses of DA and glucose were extremely weak (Fig. 4(f)). For the *in vivo* application, the biocompatibility of the coaxial fiber OECT was critical. Considering the intensity of the inflammatory response tends to decline one week after implantation [33], the coaxial fiber OECTs were implanted in the mice brains for 7 days to evaluate the biocompatibility. Glial fibrillary acidic protein (GFAP) and ionized calcium-binding adapter molecule 1 (Iba-1) were used to mark the astrocytes and microglia in the immunofluorescence staining. The fluorescence intensities of GFAP and Iba-1 in the experimental group were similar to those in the control group,

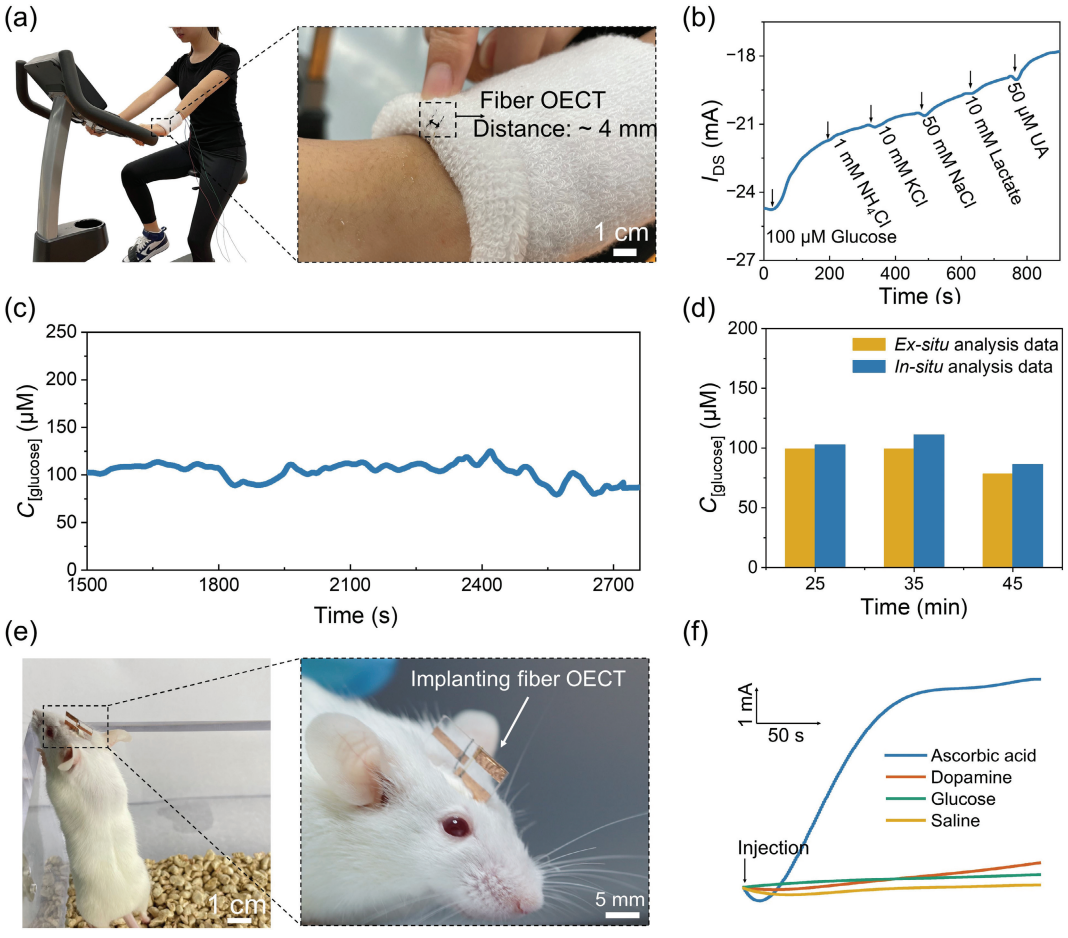

Figure 4 Wearable and implantable application of coaxial fiber OECTs. (a) Photograph of a female volunteer wearing the fiber OECT while cycling. The inset shows the fiber OECT woven into the wrister. (b) The interference study for glucose sensing of fiber OECT. (c) Real-time monitoring of glucose in sweat during cycling. (d) Comparison of *ex-situ* data from the collected sweat samples with that of the *in-situ* data after cycling for 25, 35 and 45 min. (e) Photographs of a mouse implanted with the coaxial fiber OECT at low (left) and high (right) magnifications. (f) The selectivity study for AA detection of fiber OECT *in vivo*.

indicating negligible inflammation and good biocompatibility of the coaxial fiber OECTs (Fig. S18 in the ESM)

3 Conclusion

In conclusion, by introducing the Au network as the outermost source electrode, the coaxial fiber OECT has been successfully constructed. The unique coaxial structure provides fiber OECTs with a short channel length of micrometer level and a high transconductance. Based on the modification of CNT fiber gates, the coaxial fiber OECTs demonstrate high sensitivities to different chemicals. In addition, the coaxial fiber channel and the CNT fiber gate electrodes were highly stable under deformation, friction and body fluid soaking. Coaxial fiber OECTs showed the potential in wearable and implantable applications to monitor glucose in sweat and detect AA in mice brains. This work proposed a new strategy to largely improve the transconductance of fiber OECTs and open up the avenue to high-sensitivity fiber biosensors.

4 Methods

4.1 Materials

Nylon fibers (0.18 mm) were purchased from Xinyue Co., Ltd. PEDOT:PSS aqueous dispersion (Clevious PH1000) was purchased from Heraeus Co., Ltd. KCl, NaCl, NH_4Cl, H_2O_2 (AR, 30% in H_2O), methanol, ethanol, acetone and N,N-dimethylacetamide (DMAC) were purchased from Sinopharm Chemical Reagent Co., Ltd. Glutaraldehyde (AR, 50% in H_2O), agarose, dopamine hydrochloride (DA), AA, UA, lactate, GOx (10 KU (KU = Kilo unit, 1 KU = 100 mg)), 3-glycidoxypropyltrimethoxysilane (GOPS) and K_2PtCl_6 were purchased from Sigma Aldrich Co. TTF was purchased from Shanghai Bide Pharmaceutical Technology Co., Ltd. β-D-Glucose was purchased from TCI. Waterborne acrylic resin colloidal dispersion (Steba AW F66747) was purchased from Guangdong Bangtai New Material Technology Co., Ltd. Phosphate-buffered saline (PBS) and stroke-physiological saline (SPS) were acquired from Solarbio Science and Technology Co., Ltd. Artificial cerebrospinal fluid (ACSF) was purchased from Fuzhou Phygene Biotechnology Co., Ltd. Fluorocarbon surfactant (FS-63) was purchased from Dupont Co. Polyester film was purchased from Wowking Material Co., Ltd.

4.2 Fabrication of coaxial fiber OECTs

Fabrication of channel. 5 nm Cr and 100 nm Au were deposited onto a nylon fiber as the drain electrode by thermal evaporation. To ensure complete coverage on the fiber surface, the fiber was suspended in the chamber, and gold was evaporated onto its front and back respectively. The PEDOT:PSS solution was mixed with 1 wt.% 3-glycidoxypropyltrimethoxysilane cross-linker to enhance its water stability. And 0.05 wt.% fluorocarbon surfactant was added to reduce the surface tension of PEDOT:PSS solution. In order to further improve the stability of film formation of PEDOT:PSS on the fiber surface, the PEDOT:PSS solution was concentrated by oil bath. Then the concentrated PEDOT:PSS solution was coated on the gold-plated nylon fiber by dip-coating method. In dip-coating technique, the film thickness is mainly

related to the absolute viscosity and shear rate of film-forming fluid and the number of dip-coating [59, 60]. In order to control the channel length, we specially controlled the concentration ratio of the PEDOT:PSS solution to 40% by mass to keep the solution viscosity constant. Besides, we dip-coated with concentrated PEDOT:PSS solution at a speed of 300 mm/min for 3 times. The constant dip-coating speed ensured the shear rate of PEDOT:PSS solution and the certain number of dip-coating guaranteed the number of film layers. Therefore, we controlled the channel length of around 5 μm. To enhance the conductivity of the PEDOT:PSS layer, the whole fiber was immersed into methanol for 5 min and then transferred to a glove box filled with Ar gas for post-annealing at 140 °C for 1 h. For the fabrication of the Au network source electrode, the fiber with PEDOT:PSS layer was immersed in the waterborne acrylic resin colloidal dispersion and pulled out at the speed of 300 mm/min by a universal testing machine. A crackle template was formed after drying in the air at room temperature for 10 min. After drying, 50 nm of Au layer was deposited onto the crackle template by thermal evaporation. The lift-off step was conducted by soaking the whole fiber in DMAC for 1 h and then rinsing it with ethanol. Finally, the polyester film was wrapped on the fiber as the insulating layer.

Fabrication of CNT fiber. CNT fiber was synthesized in a tube furnace at the temperature of 1200 °C by floating catalyst chemical vapor deposition with thiophene and ferrocene as catalysts, ethanol as carbon source, flowing Ar (200 standard cubic centimeters per minute (sccm)) as carrier gas and H_2 (2000 sccm) as reduction gas. The CNT fiber was pulled out of the tube furnace by a titanium rod and then passed through water and ethanol successively. It was finally dried in the air overnight [3].

Preparation of H_2O_2 sensing fiber gate. The H_2O_2 sensing fiber gate was prepared by electrochemical deposition of Pt NPs onto the CNT fiber. The platinum electroplating solution was composed of K_2PtCl_6 (1 mM) and KCl (0.1 M). The working, counter and reference electrodes were made of CNT fiber, Pt wire and Ag/AgCl, respectively. Double potential step method was repeated until electroplating 0.08 C charge by setting the first step at 0.5 V for 10 s and the second step at −0.7 V for 10 s.

Preparation of glucose sensing fiber gate. To modify the CNT fiber with TTF as electron transfer agent, the CNT fiber was immersed in the TTF solution (20 mM) for 1 h. The solvent of TTF solution was a mixture of ethanol and acetone with a volume ratio of 9:1. After drying in the air for 10 min, the CNT fiber modified with TTF was soaked in the GOx PBS solution (40 mg/mL) overnight at 4 °C. Glutaraldehyde with a 0.15% volume ratio was added to the GOx PBS solution in order to immobilize GOx on the CNT by crosslinking. To protect the glucose oxidase, the CNT/TTF/GOx fiber gate was stored in a refrigerator at 4 °C.

4.3 Characterization

The cross-section and surface morphology of fiber OECTs were characterized by field emission scanning electron microscopy (Zeiss Ultra 55). All of the electrical characterizations were done in 1× PBS solution. Output, transfer, response time and cycle stability were measured by Keithley 2614B. For the output characteristic, the V_D was set from 0 to −0.6 V and V_G was set from 0 to 0.6 V with 0.1 V step. For the transfer characteristic, the V_D was set at −0.6 V and V_G was set from 0 to 0.8 V. All the sensitivity tests were conducted in chronoamperometry by a CHI660e electrochemical workstation with applied V_D of −0.6 V and a Keithley K2400 with applied V_G of 0.2 V. For the AA sensitivity test, the fiber OECT with a bare CNT fiber gate was immersed in PBS solution added with different concentrations of AA. The response of the OECT to AA (ΔI_{DS}) was calculated by the following equation: $\Delta I_{DS} = I_{DS} - I_0$, where I_{DS} and I_0 are the drain currents of the OECT in the presence and absence of AA, respectively. Therefore, the curve of ΔI_{DS} to the common logarithm of concentration was achieved. And the sensitivity of AA was the slope value obtained by linear fitting of the curve. For the sensitivity test of H_2O_2 and glucose, similar methods were used with a H_2O_2 sensing fiber gate and glucose sensing fiber gate instead of a bare CNT fiber gate. The electrochemical stability of CNT fiber gate was tested in alternating current (A.C.) impedance with a frequency range of 1–100,000 Hz by a CHI660e electrochemical workstation. The three-electrode system was chosen with CNT fiber, Ag/AgCl and Pt wire as working, reference and counter electrodes, respectively. To characterize the mechanical stability of the CNT fiber gate, the impedance of CNT fiber was tested after bending and friction for 1000 times.

4.4 Applications

The animal experiment protocols were approved by Animal Experimentation Committee of Fudan University. And all the experimental mice were treated according to guidelines for the care and use of experimental animals set by the National Institutes of Health and Fudan University. Ten female mice (BALB/c, 6 weeks old) were purchased from Shanghai Jiesijie Experimental Animal Co., Ltd. On the 7th day after implantation of the fiber OECT, the mice were sacrificed and their brains were removed. In order to maintain the cells and structures in the brain, the brains were immersed in 4% (v/v) paraformaldehyde in 0.01 M PBS solution for 48 h. For immunofluorescence staining, neuron-specific nuclear protein (NeuN) (1:500, GB13138-1, Servicebio), GFAP (1:1000, GB11096, Servicebio) and Iba-1 (1:200, GB13105-1, Servicebio) were used as primary antibody. 488 conjugated goat anti-mouse (1:400, GB25301, Servicebio) and Cy3 conjugated goat anti-rabbit IgG (H+L) (1:300, GB21303, Servicebio) were used as secondary antibody. Finally, 4,6-diamidino-2-phenylindole dihydrochloride (DAPI) (G1012, Servicebio) was added into the brain tissue sections.

Analysis of glucose in sweat. The experiment protocols were approved by the Animal and Human Experimentation Committee of Fudan University. A healthy female subject was recruited from Fudan University and gave written, informed consent before participating in the study. For *in-situ* analysis, the fiber OECT and a glucose-sensing fiber gate with a distance of 4 mm were woven into a wrister, and connected to a CHI660e electrochemical workstation and a Keithley K2400 through the enameled wire. We chose this distance because the large distance would reduce the electric field, thus decreasing the transconductance [61, 62] while the small distance might cause the short circuit between the gate electrode and the channel. A female volunteer wore the wrister during cycling. To verify the reliability of detection, sweat samples were collected after cycling for 25, 35 and 45 min for *ex-situ* analysis. These samples were measured by the commercial glucose-sensing electrodes purchased from Shenzhen Refreshing Biosensor Technology Co., Ltd.

In vivo detection of ascorbic acid. The mouse was anesthetized with 4% isoflurane gas before the operation and 2% during the operation. A fiber OECT with a CNT fiber gate was implanted into the mouse brain with the aid of a tungsten wire. After the implantation, the detection of ascorbic acid was conducted by injecting 2 μL of AA SPS solution (5 mM) *in situ* with a microsyringe. For the *in vivo* anti-interference characterization, 2 μL of SPS solution, DA SPS solution (5 mM) and glucose SPS solution (5 mM) were successively injected into the control mouse's brain.

Acknowledgements

This work was supported by the National Natural Science

Foundation of China (NSFC, Nos. 52122310 and 22075050), Science and Technology Commission of Shanghai Municipality (STCSM, Nos. 21511104900 and 20JC1414902), China Postdoctoral Science Foundation (CPSF, Nos. VLH1717003, KLH1717015), Shanghai Municipal Science and Technology Major Project (No. 2018SHZDZX01), ZJ Lab, and Shanghai Center for Brain Science and Brain-Inspired Technology.

Electronic Supplementary Material: Supplementary material (schematic diagram and SEM of the fabrication process of the coaxial fiber OECT; optical microscopy images of Au network; electrochemical tests of the coaxial fiber OECTs and CNT fibers; SEM of CNT fibers with different modification; immunofluorescence images) is available in the online version of this article at https://doi.org/10.1007/s12274-023-5722-y.

References

[1] Wang, L.; Wang, L. Y.; Zhang, Y.; Pan, J.; Li, S. Y.; Sun, X. M.; Zhang, B.; Peng, H. S. Weaving sensing fibers into electrochemical fabric for real-time health monitoring. *Adv. Funct. Mater.* **2018**, *28*, 1804456.

[2] Yoon, J. H.; Kim, S. M.; Park, H. J.; Kim, Y. K.; Oh, D. X.; Cho, H. W.; Lee, K. G.; Hwang, S. Y.; Park, J.; Choi, B. G. Highly self-healable and flexible cable-type pH sensors for real-time monitoring of human fluids. *Biosens. Bioelectron.* **2020**, *150*, 111946.

[3] Wang, L. Y.; Xie, S. L.; Wang, Z. Y.; Liu, F.; Yang, Y. F.; Tang, C. Q.; Wu, X. Y.; Liu, P.; Li, Y. J.; Saiyin, H. et al. Functionalized helical fibre bundles of carbon nanotubes as electrochemical sensors for long-term *in vivo* monitoring of multiple disease biomarkers. *Nat. Biomed. Eng.* **2020**, *4*, 159–171.

[4] Qing, X.; Wang, Y. D.; Zhang, Y.; Ding, X. C.; Zhong, W. B.; Wang, D.; Wang, W. W.; Liu, Q. Z.; Liu, K.; Li, M. F. et al. Wearable fiber-based organic electrochemical transistors as a platform for highly sensitive dopamine monitoring. *ACS Appl. Mater. Interfaces* **2019**, *11*, 13105–13113.

[5] Yang, A. N.; Li, Y. Z.; Yang, C. X.; Fu, Y.; Wang, N. X.; Li, L.; Yan, F. Fabric organic electrochemical transistors for biosensors. *Adv. Mater.* **2018**, *30*, 1800051.

[6] Kim, Y.; Lim, T.; Kim, C. H.; Yeo, C. S.; Seo, K.; Kim, S. M.; Kim, J.; Park, S. Y.; Ju, S.; Yoon, M. H. Organic electrochemical transistor-based channel dimension-independent single-strand wearable sweat sensors. *NPG Asia Mater.* **2018**, *10*, 1086–1095.

[7] Zhang, Y.; Wang, Y. D.; Qing, X.; Wang, Y.; Zhong, W. B.; Wang, W. W.; Chen, Y. L.; Liu, Q. Z.; Li, M. F.; Wang, D. Fiber organic electrochemical transistors based on multi-walled carbon nanotube and polypyrrole composites for noninvasive lactate sensing. *Anal. Bioanal. Chem.* **2020**, *412*, 7515–7524.

[8] Wang, Y. D.; Zhou, Z.; Qing, X.; Zhong, W. B.; Liu, Q. Z.; Wang, W. W.; Li, M. F.; Liu, K.; Wang, D. Ion sensors based on novel fiber organic electrochemical transistors for lead ion detection. *Anal. Bioanal. Chem.* **2016**, *408*, 5779–5787.

[9] Wang, Y. D.; Qing, X.; Zhou, Q.; Zhang, Y.; Liu, Q. Z.; Liu, K.; Wang, W. W.; Li, M. F.; Lu, Z. T.; Chen, Y. L. et al. The woven fiber organic electrochemical transistors based on polypyrrole nanowires/reduced graphene oxide composites for glucose sensing. *Biosens. Bioelectron.* **2017**, *95*, 138–145.

[10] Rivnay, J.; Leleux, P.; Ferro, M.; Sessolo, M.; Williamson, A.; Koutsouras, D. A.; Khodagholy, D.; Ramuz, M.; Strakosas, X.; Owens, R. M. et al. High-performance transistors for bioelectronics through tuning of channel thickness. *Sci. Adv.* **2015**, *1*, e1400251.

[11] Rivnay, J.; Inal, S.; Salleo, A.; Owens, R. M.; Berggren, M.; Malliaras, G. G. Organic electrochemical transistors. *Nat. Rev. Mater.* **2018**, *3*, 17086.

[12] Liang, Y. Y.; Brings, F.; Maybeck, V.; Ingebrandt, S.; Wolfrum, B.; Pich, A.; Offenhäusser, A.; Mayer, D. Tuning channel architecture of interdigitated organic electrochemical transistors for recording the action potentials of electrogenic cells. *Adv. Funct. Mater.* **2019**, *29*, 1902085.

[13] Wu, X. Y.; Feng, J. Y.; Deng, J.; Cui, Z. C.; Wang, L. Y.; Xie, S. L.; Chen, C. R.; Tang, C. Q.; Han, Z. Q.; Yu, H. B. et al. Fiber-shaped organic electrochemical transistors for biochemical detections with high sensitivity and stability. *Sci. China Chem.* **2020**, *63*, 1281–1288.

[14] Yang, Y. X.; Wei, X. F.; Zhang, N. N.; Zheng, J. J.; Chen, X.; Wen, Q.; Luo, X. X.; Lee, C. Y.; Liu, X. H.; Zhang, X. C. et al. A non-printed integrated-circuit textile for wireless theranostics. *Nat. Commun.* **2021**, *12*, 4876.

[15] Cicoira, F.; Sessolo, M.; Yaghmazadeh, O.; DeFranco, J. A.; Yang, S. Y.; Malliaras, G. G. Influence of device geometry on sensor characteristics of planar organic electrochemical transistors. *Adv. Mater.* **2010**, *22*, 1012–1016.

[16] Lu, W. B.; Zu, M.; Byun, J. H.; Kim, B. S.; Chou, T. W. State of the art of carbon nanotube fibers: Opportunities and challenges. *Adv. Mater.* **2012**, *24*, 1805–1833.

[17] Kumar, A.; Pujar, R.; Gupta, N.; Tarafdar, S.; Kulkarni, G. U. Stress modulation in desiccating crack networks for producing effective templates for patterning metal network based transparent conductors. *Appl. Phys. Lett.* **2017**, *111*, 013502.

[18] Routh, A. F. Drying of thin colloidal films. *Rep. Prog. Phys.* **2013**, *76*, 046603.

[19] Rao, K. D. M.; Gupta, R.; Kulkarni, G. U. Fabrication of large area, high-performance, transparent conducting electrodes using a spontaneously formed crackle network as template. *Adv. Mater. Interfaces* **2014**, *1*, 1400090.

[20] Kim, Y. G.; Tak, Y. J.; Park, S. P.; Kim, H. J.; Kim, H. J. Structural engineering of metal-mesh structure applicable for transparent electrodes fabricated by self-formable cracked template. *Nanomaterials* **2017**, *7*, 214.

[21] Tao, Y.; Wang, Y.; Zhu, R. F.; Chen, Y. L.; Liu, X.; Li, M. F.; Yang, L. Y.; Wang, Y. D.; Wang, D. Fiber based organic electrochemical transistor integrated with molecularly imprinted membrane for uric acid detection. *Talanta* **2022**, *238*, 123055.

[22] Xi, X.; Wu, D. Q.; Ji, W.; Zhang, S. N.; Tang, W.; Su, Y. Z.; Guo, X. J.; Liu, R. L. Manipulating the sensitivity and selectivity of OECT-based biosensors via the surface engineering of carbon cloth gate electrodes. *Adv. Funct. Mater.* **2020**, *30*, 1905361.

[23] Bernards, D. A.; Macaya, D. J.; Nikolou, M.; DeFranco, J. A.; Takamatsu, S.; Malliaras, G. G. Enzymatic sensing with organic electrochemical transistors. *J. Mater. Chem.* **2008**, *18*, 116–120.

[24] Lykkesfeldt, J.; Tveden-Nyborg, P. The pharmacokinetics of vitamin C. *Nutrients* **2019**, *11*, 2412.

[25] Tolosa, V. M.; Wassum, K. M.; Maidment, N. T.; Monbouquette, H. G. Electrochemically deposited iridium oxide reference electrode integrated with an electroenzymatic glutamate sensor on a multi-electrode arraymicroprobe. *Biosens. Bioelectron.* **2013**, *42*, 256–260.

[26] Demuru, S.; Huang, C. H.; Parvez, K.; Worsley, R.; Mattana, G.; Piro, B.; Noël, V.; Casiraghi, C.; Briand, D. All-inkjet-printed graphene-gated organic electrochemical transistors on polymeric foil as highly sensitive enzymatic biosensors. *ACS Appl. Nano Mater.* **2022**, *5*, 1664–1673.

[27] Ohayon, D.; Nikiforidis, G.; Savva, A.; Giugni, A.; Wustoni, S.; Palanisamy, T.; Chen, X. X.; Maria, I. P.; Di Fabrizio, E.; Costa, P. M. F. J. et al. Biofuel powered glucose detection in bodily fluids with an n-type conjugated polymer. *Nat. Mater.* **2020**, *19*, 456–463.

[28] Chen, C.; Xie, Q. J.; Yang, D. W.; Xiao, H. L.; Fu, Y. C.; Tan, Y. M.; Yao, S. Z. Recent advances in electrochemical glucose biosensors: A review. *RSC Adv.* **2013**, *3*, 4473–4491.

[29] Zafar, H.; Channa, A.; Jeoti, V.; Stojanović, G. M. Comprehensive review on wearable sweat-glucose sensors for continuous glucose monitoring. *Sensors* **2022**, *22*, 638.

[30] Ait Yazza, A.; Blondeau, P.; Andrade, F. J. Simple approach for building high transconductance paper-based organic electrochemical transistor (OECT) for chemical sensing. *ACS Appl. Electron. Mater.* **2021**, *3*, 1886–1895.

[31] Sonner, Z.; Wilder, E.; Heikenfeld, J.; Kasting, G.; Beyette, F.; Swaile, D.; Sherman, F.; Joyce, J.; Hagen, J.; Kelley-Loughnane, N. et al. The microfluidics of the eccrine sweat gland, including biomarker partitioning, transport, and biosensing implications. *Biomicrofluidics* **2015**, *9*, 031301.

[32] Zhao, J. Q.; Lin, Y. J.; Wu, J. B.; Nyein, H. Y. Y.; Bariya, M.; Tai, L. C.; Chao, M. H.; Ji, W. B.; Zhang, G.; Fan, Z. Y. et al. A fully integrated and self-powered smartwatch for continuous sweat glucose monitoring. *ACS Sens.* **2019**, *4*, 1925–1933.
[33] Tang, C. Q.; Xie, S. L.; Wang, M. Y.; Feng, J. Y.; Han, Z. Q.; Wu, X. Y.; Wang, L. Y.; Chen, C. R.; Wang, J. J.; Jiang, L. P. et al. A fiber-shaped neural probe with alterable elastic moduli for direct implantation and stable electronic-brain interfaces. *J. Mater. Chem. B* **2020**, *8*, 4387–4394.
[34] Janzakova, K.; Ghazal, M.; Kumar, A.; Coffinier, Y.; Pecqueur, S.; Alibart, F. Dendritic organic electrochemical transistors grown by electropolymerization for 3D neuromorphic engineering. *Adv. Sci.* **2021**, *8*, 2102973.
[35] Fang, B.; Yan, J. M.; Chang, D.; Piao, J.; Ma, K. M.; Gu, Q.; Gao, P.; Chai, Y.; Tao, X. M. Scalable production of ultrafine polyaniline fibres for tactile organic electrochemical transistors. *Nat. Commun.* **2022**, *13*, 2101.
[36] Zhang, L. S.; Andrew, T. Vapor-coated monofilament fibers for embroidered electrochemical transistor arrays on fabrics. *Adv. Electron. Mater.* **2018**, *4*, 1800271.
[37] Sarabia-Riquelme, R.; Andrews, R.; Anthony, J. E.; Weisenberger, M. C. Highly conductive wet-spun PEDOT: PSS fibers for applications in electronic textiles. *J. Mater. Chem. C* **2020**, *8*, 11618–11630.
[38] Hofmann, A. I.; Östergren, I.; Kim, Y.; Fauth, S.; Craighero, M.; Yoon, M. H.; Lund, A.; Müller, C. All-polymer conducting fibers and 3D prints via melt processing and templated polymerization. *ACS Appl. Mater. Interfaces* **2020**, *12*, 8713–8721.
[39] Shi, Z. N.; Xu, Z.; Hu, J.; Wei, W. W.; Zeng, X. R.; Zhao, W. W.; Lin, P. Ascorbic acid-mediated organic photoelectrochemical transistor sensing strategy for highly sensitive detection of heart-type fatty acid binding protein. *Biosens. Bioelectron.* **2022**, *201*, 113958.
[40] Tang, K.; Turner, C.; Case, L.; Mehrehjedy, A.; He, X. Y.; Miao, W. J.; Guo, S. Organic electrochemical transistor with molecularly imprinted polymer-modified gate for the real-time selective detection of dopamine. *ACS Appl. Polym. Mater.* **2022**, *4*, 2337–2345.
[41] Zhang, M.; Liao, C. Z.; Yao, Y. L.; Liu, Z. K.; Gong, F. F.; Yan, F. High-performance dopamine sensors based on whole-graphene solution-gated transistors. *Adv. Funct. Mater.* **2014**, *24*, 978–985.
[42] Liao, C. Z.; Zhang, M.; Niu, L. Y.; Zheng, Z. J.; Yan, F. Organic electrochemical transistors with graphene-modified gate electrodes for highly sensitive and selective dopamine sensors. *J. Mater. Chem. B* **2014**, *2*, 191–200.
[43] Gualandi, I.; Marzocchi, M.; Achilli, A.; Cavedale, D.; Bonfiglio, A.; Fraboni, B. Textile organic electrochemical transistors as a platform for wearable biosensors. *Sci. Rep.* **2016**, *6*, 33637.
[44] Zhang, L. J.; Wang, G. H.; Wu, D.; Xiong, C.; Zheng, L.; Ding, Y. S.; Lu, H. B.; Zhang, G. B.; Qiu, L. Z. Highly selective and sensitive sensor based on an organic electrochemical transistor for the detection of ascorbic acid. *Biosens. Bioelectron.* **2018**, *100*, 235–241.
[45] Gualandi, I.; Scavetta, E.; Mariani, F.; Tonelli, D.; Tessarolo, M.; Fraboni, B. All poly(3, 4-ethylenedioxythiophene) organic electrochemical transistor to amplify amperometric signals. *Electrochim. Acta* **2018**, *268*, 476–483.
[46] Wang, L.; Sun, Q. Z.; Zhang, L. R.; Wang, J.; Ren, G. Z.; Yu, L. Y. Z.; Wang, K. L.; Zhu, Y. M.; Lu, G.; Yu, H. D. Realizing ultrahigh transconductance in organic electrochemical transistor by Co-doping PEDOT: PSS with ionic liquid and dodecylbenzenesulfonate. *Macromol. Rapid Commun.* **2022**, *43*, 2200212.
[47] Tan, S. T. M.; Giovannitti, A.; Melianas, A.; Moser, M.; Cotts, B. L.; Singh, D.; McCulloch, I.; Salleo, A. High-gain chemically gated organic electrochemical transistor. *Adv. Funct. Mater.* **2021**, *31*, 2010868.
[48] Liao, C. Z.; Mak, C.; Zhang, M.; Chan, H. L. W.; Yan, F. Flexible organic electrochemical transistors for highly selective enzyme biosensors and used for saliva testing. *Adv. Mater.* **2015**, *27*, 676–681.
[49] Zhang, M.; Liao, C. Z.; Mak, C. H.; You, P.; Mak, C. L.; Yan, F. Highly sensitive glucose sensors based on enzyme-modified whole-graphene solution-gated transistors. *Sci. Rep.* **2015**, *5*, 8311.
[50] Guo, X.; Cao, Q. Q.; Liu, Y. W.; He, T.; Liu, J. W.; Huang, S.; Tang, H.; Ma, M. Organic electrochemical transistor for *in situ* detection of H_2O_2 released from adherent cells and its application in evaluating the in vitro cytotoxicity of nanomaterial. *Anal. Chem.* **2020**, *92*, 908–915.
[51] Strakosas, X.; Donahue, M. J.; Hama, A.; Braendlein, M.; Huerta, M.; Simon, D. T.; Berggren, M.; Malliaras, G. G.; Owens, R. M. Biostack: Nontoxic metabolite detection from live tissue. *Adv. Sci.* **2022**, *9*, 2101711.
[52] Fan, J. X.; Forero Pico, A. A.; Gupta, M. A functionalization study of aerosol jet printed organic electrochemical transistors (OECTs) for glucose detection. *Mater. Adv.* **2021**, *2*, 7445–7455.
[53] Lin, B. J.; Wang, M.; Zhao, C.; Wang, S. J.; Chen, K.; Li, X.; Long, Z. S.; Zhao, C. X.; Song, X. Y.; Yan, S. et al. Flexible organic integrated electronics for self-powered multiplexed ocular monitoring. *npj Flex. Electron.* **2022**, *6*, 77.
[54] Pappa, A. M.; Curto, V. F.; Braendlein, M.; Strakosas, X.; Donahue, M. J.; Fiocchi, M.; Malliaras, G. G.; Owens, R. M. Organic transistor arrays integrated with finger-powered microfluidics for multianalyte saliva testing. *Adv. Healthc. Mater.* **2016**, *5*, 2295–2302.
[55] Strakosas, X.; Huerta, M.; Donahue, M. J.; Hama, A.; Pappa, A. M.; Ferro, M.; Ramuz, M.; Rivnay, J.; Owens, R. M. Catalytically enhanced organic transistors for *in vitro* toxicology monitoring through hydrogel entrapment of enzymes. *J. Appl. Polym. Sci.* **2017**, *134*, 44483.
[56] Wustoni, S.; Savva, A.; Sun, R. F.; Bihar, E.; Inal, S. Enzyme-free detection of glucose with a hybrid conductive gel electrode. *Adv. Mater. Interfaces* **2019**, *6*, 1800928.
[57] Gualandi, I.; Tessarolo, M.; Mariani, F.; Arcangeli, D.; Possanzini, L.; Tonelli, D.; Fraboni, B.; Scavetta, E. Layered double hydroxide-modified organic electrochemical transistor for glucose and lactate biosensing. *Sensors* **2020**, *20*, 3453.
[58] Diacci, C.; Abedi, T.; Lee, J. W.; Gabrielsson, E. O.; Berggren, M.; Simon, D. T.; Niittylä, T.; Stavrinidou, E. Diurnal *in vivo* xylem sap glucose and sucrose monitoring using implantable organic electrochemical transistor sensors. *iScience* **2021**, *24*, 101966.
[59] Meza, B. E.; Peralta, J. M.; Zorrilla, S. E. Rheological properties of a commercial food glaze material and their effect on the film thickness obtained by dip coating. *J. Food Process Eng.* **2015**, *38*, 510–516.
[60] Sapcharoenkun, C.; Klamchuen, A.; Kasamechonchung, P.; Iemsam-Arng, J. Role of rheological behavior of sunscreens containing nanoparticles on thin film preparation. *Mater. Sci. Eng. :B* **2020**, *259*, 114608.
[61] Ferro, L. M. M.; Merces, L.; de Camargo, D. H. S.; Bof Bufon, C. C. Ultrahigh-gain organic electrochemical transistor chemosensors based on self-curled nanomembranes. *Adv. Mater.* **2021**, *33*, 2101518.
[62] Bai, L. M.; Elósegui, C. G.; Li, W. Q.; Yu, P.; Fei, J. J.; Mao, L. Q. Biological applications of organic electrochemical transistors: Electrochemical biosensors and electrophysiology recording. *Front. Chem.* **2019**, *7*, 313.